Engineering Structures 296 (2023) 116898

Contents lists available at ScienceDirect

Engineering Structures

journal homepage: www.elsevier.com/locate/engstruct

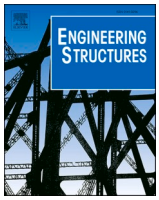

Behavior of grouted splice sleeve connection using FRP sheet

Kiarash Koushfar [a], Ahmad Baharuddin Abd. Rahman [a], Seyed Jamal Aldin Hosseini [b], Sung-Hyun Kim [c,**], Lila Soufia [a], Yusof Ahmad [a], Su-Min Kang [c], Yun Zhou [d,e,f], Jong-Min Lee [b], Hyeon-Jong Hwang [b,*]

[a] Faculty of Civil Engineering, Universiti Teknologi Malaysia, Johor, Malaysia
[b] School of Architecture, Konkuk University, Seoul, 05029, South Korea
[c] School of Architecture, Soongsil Univ, Seoul, 06978, South Korea
[d] Key Laboratory for Damage Diagnosis of Engineering Structures of Hunan Province, Hunan University, Changsha 410082, China
[e] College of Civil Engineering, Hunan University, Changsha 410082, China
[f] Key Laboratory of Building Safety and Energy Efficiency of the Ministry of Education, Hunan University, Changsha 410082, China

ARTICLE INFO

Keywords:
CFRP
GFRP
Grouted splice
Sleeve connector
Bond strength
Confinement effect

ABSTRACT

Most existing studies on grouted splice connections have focused on the bond behavior between connected steel rebars and conventional steel or iron sleeves. These research findings cannot properly predict the bond behavior and performance of the grouted splice connections, particularly when a new splice device, such as fiber reinforced polymer (FRP) materials, are adopted. The main purpose of this study is to investigate the feasibility of the proposed grouted splice sleeve connection (GSSC) using sheet materials of carbon fiber reinforced polymer (CFRP) and glass fiber reinforced polymer (GFRP). A total of 45 GSSC specimens with various rebar embedded lengths and different polymer sleeve materials were tested to failure under incremental axial pull-out load to evaluate the bond performance of the connected steel rebars in confined grout provided by the FRP sleeves. To evaluate the confinement effect of FRP sleeves on the tensile strength of the grouted connection, an analytical model was developed. The pull-out test results showed that the rebar embedded length was the major parameter affecting the average tensile strength of the GSSC. Also, the effects of mechanical properties of FRP sheets, such as the number of FRP layers and type of FRP sheets, contributed to the tensile strength of the GSSC sleeves that allow the transmission of tensile load between rebars through the medium of grout, aluminum tube, and FRP sheets. The analytical model that incorporates the confinement effects predicted well the experimental ultimate tensile strength of GSSC connections.

1. Introduction

The overall structural integrity of precast concrete (PC) structures is significantly governed by the structural performance of connections, which are the most important components in PC systems. Connections can dictate the type of frame in the precast system, the limitations of the frame, and the erection process, which emphasize the importance of connections [1,2]. Thus, the effectiveness of PC connections in transferring the forces between structural members needs to be clearly investigated. The effectiveness of the grouted splice sleeve connection (GSSC), which is generally used in practical PC design, significantly depends on the development of bond between rebars and surrounding grout. Thus, the splice connections should be able to provide structural continuity by developing adequate bar bond strength in short development length.

In grouted sleeve connections, various design parameters affect the bond strength between deformed bars and surrounding concrete, such as the embedment length of rebar, rebar diameter, rebar profile, rebar spacing, rebar casting position, concrete strength, rebar yield strength, cover concrete thickness, and confinement [3,4]. Confinement pressure is one of the main factors that improve the bond performance between rebars and surrounding concrete [5–10]. Various methods have been proposed to provide the confinement by surrounding the anchorage length of the rebar with different materials, such as transverse reinforcement [9], cylindrical steel pipes [10,11], aluminum tubes [12], spiral bars [13–17], and fiber reinforced polymer (FRP) [18]. Note that

* Corresponding authors.
** Co-corresponding author.
E-mail addresses: jangson@snu.ac.kr (S.-H. Kim), hwanggun85@naver.com (H.-J. Hwang).

https://doi.org/10.1016/j.engstruct.2023.116898
Received 10 April 2023; Received in revised form 4 September 2023; Accepted 13 September 2023
Available online 20 September 2023

the cylindrical steel pipes, aluminum tubes, and FRP materials are used to resist the splitting expansion of the bond materials surrounding the rebars, while the spiral bars and transverse reinforcement are used to restrain the propagation of splitting cracks. As the embedded length and confinement are two factors governing the feasibility of the GSSC [19], the present study focused on the effects of embedded length and confinement on the bond performance of spliced bars in the GSSC with two sleeve materials (i.e., GFRP and CFRP).

Current design codes provide limited information for the design of the GSSC due to the proprietary and confidential nature of these products. On the other hand, existing studies addressing the performance of the spliced connections are limited to small-scale tests [20–22]. Further, most of the existing studies mainly focused on GSSC using steel pipes. However, steel pipes cannot generate the required interlocking mechanism between their inner surface and grout. Thus, additional methods (e.g., welding) are needed to provide adequate interlocking mechanism [13,14,19].

Low weight and a wide variety of mechanical properties are considered as important factors in several existing studies [23–28] of the continuous fiber reinforcements. The combination of fiber reinforcements and metals including aluminum had led to the emergence of composite materials (e.g., fiber-metal laminates (FML)). These laminates are fabricated by combining the metal layers with different orientation of fiber reinforcements embedded in the resin adhesive [29–37]. The FML composites behave as a metallic structure, and show superior mechanical properties, such as excellent corrosion resistance, high fire resistance, high impact resistance, and light weight [38]. For example, the glass fiber reinforced polymer (GFRP) based FML exhibits excellent impact resistance, which is greater than that of carbon laminates and monolithic aluminum alloys [39]. Various preparation methods, such as pre-treatment by phosphoric and chromic acid for industrial tools, and materials were proposed to enhance the bond strength between fiber-aluminum layers and consequently the mechanical properties of FMLs [40].

In the present study, axial pull-out tests were performed to investigate the effect of confinement and rebar embedded length on the feasibility of grouted FRP sleeve connections under incremental axial loads. As the major test parameter, sleeves with several numbers of CFRP or GFRP layers were applied to spliced bars to generate confinement stress along the bar splices. In addition, the rebar embedded length was considered as the second parameter to evaluate the minimum rebar embedment length to ensure the rebar fracture. Based on the test results, a design model to predict the bond behavior of the proposed GSSC was developed.

2. Test plan

2.1. Test specimens

To investigate the bond performance of the GSSC with three types of sleeves (i.e., aluminum tube sleeve, carbon FRP sleeve, and glass FRP sleeve), a series of pull-out tests were carried out. Fig. 1 shows the test specimens. The test parameters were the type of sleeve (i.e., aluminum tube, and aluminum sleeve wrapped with FRP sheets), material (i.e., aluminum, carbon FRP, and glass FRP), embedded length of spliced bar (i.e., (75, 125, and 175) mm), and the number of layers (i.e., 6 and 7 layers).

Three controlled specimens, K-F, were tested under tensile load to reach their ultimate tensile strengths. In specimen groups K-F, two 500 mm Y16 reinforcing bars were used as a benchmark for the ideal grouted splice. A flexible corrugated aluminum tube with thickness of 1.0 mm was used as the sleeve (see Fig. 1(a)). The embedded lengths of spliced bars were l_e = (75, 125, and 175) mm in each group K-F. Table 1 shows the design parameters of the F-FRP specimens.

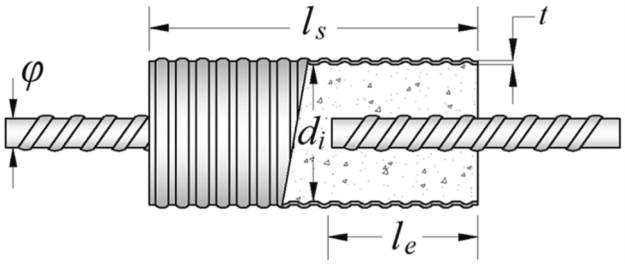

(a) Flexible corrugated aluminum tube (K-F)

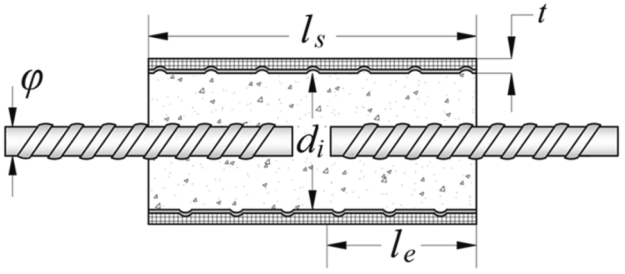

(b) Flexible corrugated aluminum sleeve wrapped with FRP sheets (F-FRP)

Fig. 1. Dimensions of sleeve connection specimens.

2.2. Preparation of sleeves

Fig. 2 shows the corrugated aluminum tube, GFRP, and CFRP sheets employed for making FRP sleeves. The F-FRP sleeves were fabricated by wrapping FRP layers around the flexible corrugated aluminum tube (Fig. 3). Based on the preliminary studies [41,42], six and seven layers of GFRP or CFRP sheets were used to avoid premature fracture of FRP sheets in F-FRP GSSC. As the test parameters, the FRP material types (i.e., carbon fibers (F-C) and glass fibers (F-G)), the number of FRP layers (i.e., 6 and 7), and bar embedment lengths (i.e., (75, 125, and 175) mm) were addressed. Fig. 4 shows the FRP sleeves manufactured for GSSC connections.

2.3. Reinforcing bars

For reinforcing bars, two 500 mm long Y16 rebars (where Y denotes the specified yield strength of 460 MPa and 16 denotes the rebar diameter of 16 mm) were used for each grouted splice. Single ends of pairs of rebars were spliced together, with an end-to-end spacing of 10 mm in sleeve, while the other ends were free. Fig. 5 shows the geometrical properties of Y16 rebar, where the rebar diameter is 16 mm, rib height of 1 mm, rib spacing of 11 mm, and rib inclination of 60°. Rebars were spliced together with Sika Grout-215 inside the sleeve. Fig. 6 and Table 2 show the material properties of Y16 rebars obtained from the rebar tensile tests.

2.4. Preparation of GSSC

For the grouting of splice sleeve connections, Sika Grout-215 (i.e., specified compressive strength of higher than 60 MPa at 28 days) was used as the bond material in the GSSC. Sika Grout-215 was prepared in accordance with the instructions provided by the manufacturer (i.e., 25 kg of grout in 4 L of water).

The present study used an unsaturated epoxy resin EPICOTE 1006 SYSTEM produced by Wee Tee Tong Chemicals Pte Ltd., Singapore. The resin ingredient was mixed under room environment, according to the

Table 1
Design parameters of specimens.

Specimens*	Number of Specimens	Materials	Number of layers	d_b (mm)	l_e (mm)	l_s (mm)	t^{**} (mm)	d_i (mm)
K-FL_{75}	3	Flexible aluminum	–	16	75	160	1.0	37
K-FL_{125}	3	Flexible aluminum	–	16	125	260	1.0	37
K-FL_{175}	3	Flexible aluminum	–	16	175	360	1.0	37
F-C_6L_{75}	3	Carbon FRP	6	16	75	160	4.0	42
F-C_6L_{125}	3	Carbon FRP	6	16	125	260	4.0	42
F-C_6L_{175}	3	Carbon FRP	6	16	175	360	4.0	42
F-C_7L_{75}	3	Carbon FRP	7	16	75	160	4.5	42
F-C_7L_{125}	3	Carbon FRP	7	16	125	260	4.5	42
F-C_7L_{175}	3	Carbon FRP	7	16	175	360	4.5	42
F-G_6L_{75}	3	Glass FRP	6	16	75	160	4.0	42
F-G_6L_{125}	3	Glass FRP	6	16	125	260	4.0	42
F-G_6L_{175}	3	Glass FRP	6	16	175	360	4.0	42
F-G_7L_{75}	3	Glass FRP	7	16	75	160	4.5	42
F-G_7L_{125}	3	Glass FRP	7	16	125	260	4.5	42
F-G_7L_{175}	3	Glass FRP	7	16	175	360	4.5	42

* L75, L125, and L175 indicate the embedded lengths (*le*) of 75 mm, 125 mm, and 175 mm, respectively.
**The thickness of aluminum tube in all specimens is 1.0 mm, and each of them is corrugated.

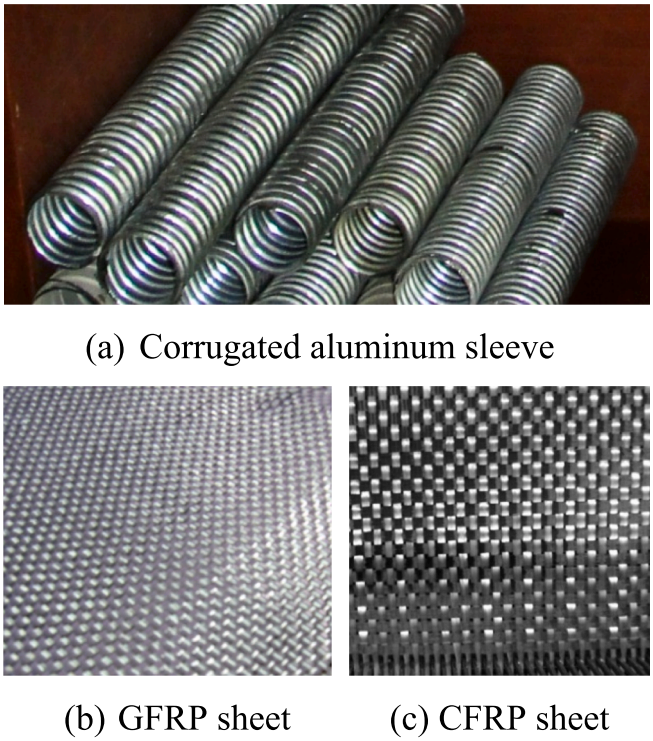

Fig. 2. Materials for FRP sleeves.

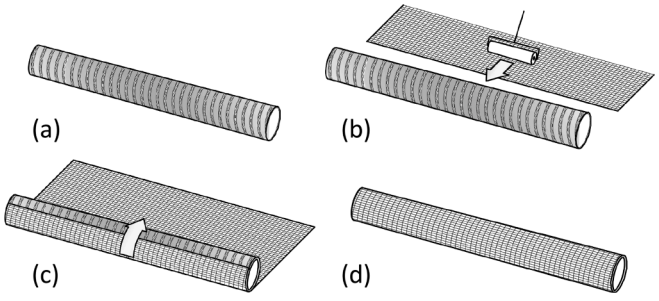

Fig. 3. Preparation of G-FRP and C-FRP sleeves: (a) Corrugated aluminum tube; (b) Applying epoxy resin on the FRP sheets; (c) Wrapping of aluminum tube with FRP sheets; (d) FRP sleeve.

Fig. 4. G-FRP and C-FRP sleeves for GSSC connections.

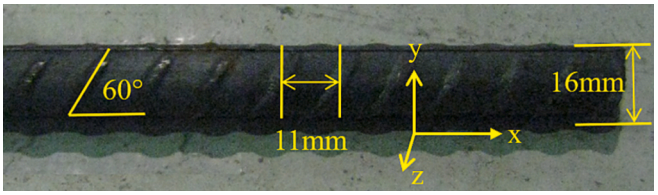

Fig. 5. Geometrical properties of Y16 rebar.

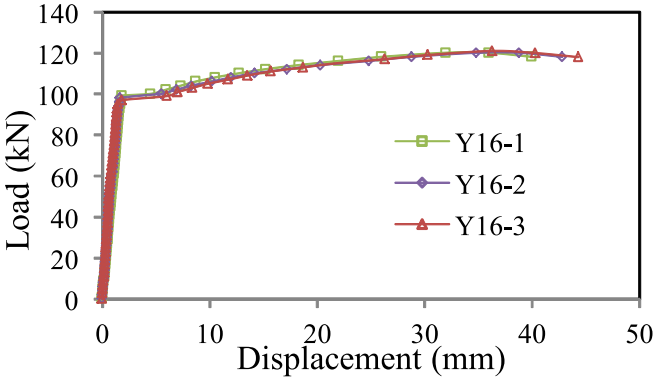

Fig. 6. Load-displacement responses of Y16 rebar.

manufacturer's specifications. The resin was pigmented by the addition of up to 60% EPICOTE 1006 Hardener Part B. Table 3 shows the mechanical and physical properties of the mixture as specified by the manufacturer for the pultrusion process.

In this study, continuous woven roving E-glass and carbon fiber with

Table 2
Material properties of Y16 reinforcing bars.

Specimen	Yield strength (MPa)	Ultimate tensile strength (MPa)	Elongation (mm)
Y16-1	503	601	32.6
Y16-2	500	597	34.8
Y16-3	493	595	36.3

Table 3
Mechanical and Physical Properties of the EPICOTE 1006 SYSTEM.

Pencil strength	2H–3H
Compressive strength	82 N/mm^2
Tensile strength	30 N/mm^2
Heat distortion	100 °C
Elongation	1.9%
Gel time (at 150 g mass at 20 °C)	67 min
Pot life (at 150 g mass at 20 °C)	47 min

density of 300 g/m^2 was used. The fibers were compatible with the resin as recommended by the manufacturer. Similar to glass fiber, continuous woven roving carbon fiber was used. Table 4 shows the material properties of the woven roving fibers of GFRP and CFRP provided by manufacturer, and CFRP and GFRP coupons. Monotonic tensile tests were performed on five CFRP and GFRP coupon specimens with the dimensions of (25 × 250 × 2.5) mm to measure the tensile properties of the composite materials (see Fig. 7). Note that the configuration of the tensile test for FRP composite materials satisfied the requirements of ASTM D3039/D3039M-14 [43].

2.5. Advantages and applications of the proposed GSSC

FRP sheet has the advantage of excellent tensile strength (Table 4). On the other hand, the aluminum corrugated sleeve is weak in tension but has excellent corrugated profile inside the sleeve. Thus, a combination of FRP sheets and aluminum corrugated profile can provide the tension resistance and shear keys for bearing resistance for GSSC (see Fig. 8).

The pull-out test results of the proposed GSSC under axial loads are applicable to evaluate the behavior and performance of the sleeve connections under monotonic loading, but cannot be extrapolated to different loading conditions, such as cyclic or dynamic loading. However, the pull-out test results would be applicable to evaluate the behavior and performance of connections in a beam under flexural loading, because the flexural test results show similar trend to those of the direct pull-out tests [16].

In terms of manufacturing cost, compared to conventional cast iron couplers that require special equipment, the proposed GSSC only requires FRP sheets, epoxy resin, and corrugated aluminum tube, and can be manufactured without any sophisticated equipment (see Figs. 3 and 4). Thus, the proposed GSSC with short rebar embedment length and cost effectiveness can be employed in precast concrete column-to-column or wall-to-wall connections [16].

Table 4
Specification of woven roving FRP fibers.

Properties of FRP sheet	Specification of manufacturer		Coupon test	
	Woven roving E-glass fibers GFRP	Woven roving carbon fibers CFRP	GFRP	CFRP
Standard weight (g/m^2)	300	300	–	
Tensile strength (MPa)	980–1,470	4,900	700	1,200
Elastic modulus (MPa)	51,000	230,000	29,000	125,000
Maximum elongation (%)	3	1.9	–	–

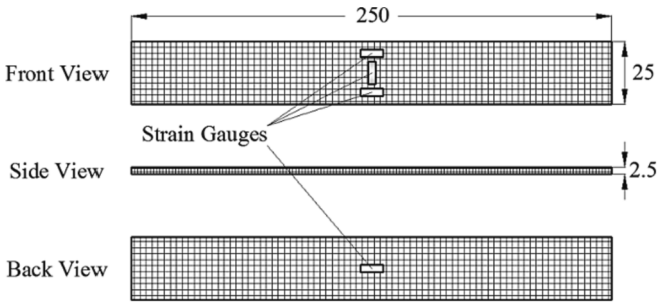

Fig. 7. CFRP and GFRP composite coupons.

Fig. 8. GSSC specimens with GFRP sheets for pull-out tests.

2.6. Pull-out test

Fig. 9 shows the test setup and instrumentation of measurement. To perform the pull-out test, the loading procedure was conducted according to the recommendations of AC-133 [44] and ASTM A1034A [45]. The tests were performed under axial tension-pullout load by using a hydraulic actuator with a loading rate of 0.5 kN/s, until the specimen failed under incremental tensile load.

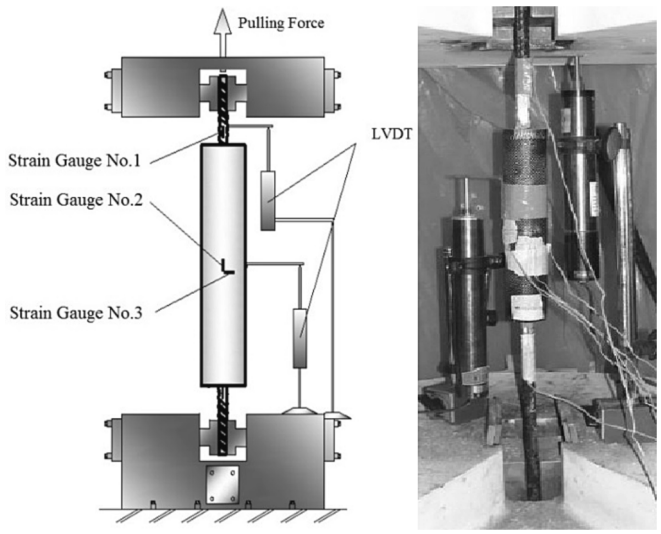

Fig. 9. Pull-out test setup.

To measure the vertical displacement of the specimens, two linear variable displacement transducers (LVDTs) were installed on the rebar and sleeve of the specimens. During the pull-out test, slip displacement occurs due to several factors, including the bond-slip between rebar and surrounding grout, tension elongation of sleeve, bond-slip between grout and sleeve, and gripping slip of the actuator. Thus, the displacements of the rebar and sleeve were measured by the two LVDTs to evaluate the slip.

Three strain gauges were installed on the sleeves and spliced bars according to the recommendations of ASTM standard [45] (see Fig. 9). To investigate the tensile strain of the spliced bars, strain gauge No. 1 was longitudinally attached to the rebar at a distance of one bar diameter (i.e., 16 mm) from the top end of the sleeve. Strain gauge No. 2 was longitudinally attached to the middle of the sleeve to measure the longitudinal strain. Strain gauge No. 3 was transversely attached to the middle of the sleeve to measure the transverse strain.

3. Test results

3.1. Control specimens

Table 5 shows the results of the tensile load tests for GSSC specimens. The test results showed that the effect of rebar embedded length on the ultimate tensile strength was insignificant in the control specimen groups K-F. This is because sufficient interlocking mechanism and confinement were not provided by the corrugated aluminum tubes. As shown in Table 5, although the control specimen groups K-F (using flexible aluminum sleeve) had excellent corrugated profile, they exhibited the lowest tensile strengths among the grouted splices. Ultimately, fracture of the sleeve occurred at the discontinuity of the spliced bars due to the insufficient cross-sectional area (i.e., thickness of 1.0 mm) and low tensile strength of the corrugated sleeve.

3.2. Failure modes of the grouted splice sleeves

In the test specimens, four major failure modes were bar fracture, bar bond–slip, aluminum tube bond–slip, and FRP sleeve fracture. In all specimens, the tensile capacity of the grouted splice FRP sleeve was

Table 5
Results of tensile load tests for the F-FRP grouted splices.

*Specimen	Yield strength		Yield displacement		Tensile strength		Ultimate displacement		Failure mode
	P_y (kN)	Average (Std.error)	Δ_y (mm)	Average (Std.error)	P_u(kN)	Average (Std.error)	Δ_u (mm)	Average (Std.error)	
K-FL$_{75}$-1	–	–	–	–	25.2	24.7	0.79	0.68	Sleeve Fracture
K-FL$_{75}$-2	–		–		24.6	(0.37)	0.63	(0.08)	Sleeve Fracture
K-FL$_{75}$-3	–		–		24.3		0.61		Sleeve Fracture
K-FL$_{125}$-1	–	–	–	–	26.4	26.1	0.89	0.84	Sleeve Fracture
K-FL$_{125}$-2	–		–		25.7	(0.29)	0.79	(0.04)	Sleeve Fracture
K-FL$_{125}$-3	–		–		26.1		0.83		Sleeve Fracture
K-FL$_{175}$-1	–	–	–	–	29.7	29.0	1.01	0.93	Sleeve Fracture
K-FL$_{175}$-2	–		–		28.5	(0.50)	0.88	(0.06)	Sleeve Fracture
K-FL$_{175}$-3	–		–		28.9		0.90		Sleeve Fracture
F-C$_6$L$_{75}$-1	70.1	68.7	2.08	2.09	70.1	68.7	2.25	2.17	Bar bond slip
F-C$_6$L$_{75}$-2	73.1	(4.28)	2.27	(0.15)	73.1	(4.28)	2.33	(0.17)	Bar bond slip
F-C$_6$L$_{75}$-3	62.9		1.91		62.9		1.94		Bar bond slip
F-C$_6$L$_{125}$-1	99.1	101.1	3.42	3.09	99.1	101.1	3.96	4.07	Sleeve Fracture
F-C$_6$L$_{125}$-2	101.3	(1.56)	2.87	(0.24)	101.3	(1.56)	4.82	(0.57)	Sleeve Fracture
F-C$_6$L$_{125}$-3	102.9		2.99		102.9		3.43		Sleeve Fracture
F-C$_6$L$_{175}$-1	98.9	95.8	2.42	2.41	114.8	115.4	25.77	21.79	Bar Fracture
F-C$_6$L$_{175}$-2	93.6	(2.26)	2.53	(0.11)	113.8	(1.56)	21.95	(3.31)	Bar Fracture
F-C$_6$L$_{175}$-3	94.9		2.27		117.5		17.66		Bar Fracture
F-C$_7$L$_{75}$-1	68.5	70.4	2.00	2.06	68.5	70.4	2.16	2.22	Bar bond slip
F-C$_7$L$_{75}$-2	74.2	(2.71)	2.13	(0.05)	74.2	(2.71)	2.34	(0.09)	Bar bond slip
F-C$_7$L$_{75}$-3	68.4		2.06		68.4		2.15		Bar bond slip
F-C$_7$L$_{125}$-1	105.0	102.2	2.20	2.31	105.0	104.7	8.95	8.63	Bar bond slip
F-C$_7$L$_{125}$-2	95.1	(5.03)	2.54	(0.16)	102.7	(1.53)	8.83	(0.37)	Bar bond slip
F-C$_7$L$_{125}$-3	106.4		2.19		106.4		8.12		Bar bond slip
F-C$_7$L$_{175}$-1	95.6	95.4	2.61	2.70	115.8	117.2	24.51	23.98	Bar Fracture
F-C$_7$L$_{175}$-2	93.9	(1.11)	2.64	(0.11)	116.6	(1.50)	26.66	(2.43)	Bar Fracture
F-C$_7$L$_{175}$-3	96.6		2.85		119.3		20.77		Bar Fracture
F-G$_6$L$_{75}$-1	60.1	59.2	1.79	1.70	60.1	59.2	1.83	1.82	Bar bond slip
F-G$_6$L$_{75}$-2	56.4	(2.02)	1.75	(0.10)	56.4	(2.02)	1.79	(0.02)	Bar bond slip
F-G$_6$L$_{75}$-3	61.1		1.55		61.1		1.83		Bar bond slip
F-G$_6$L$_{125}$-1	89.0	89.1	2.55	2.52	89.0	89.1	2.82	2.92	A tube bond slip
F-G$_6$L$_{125}$-2	90.2	(0.90)	2.38	(0.10)	90.2	(0.90)	2.91	(0.09)	A tube bond slip
F-G$_6$L$_{125}$-3	88.0		2.63		88.0		3.03		A tube bond slip
F-G$_6$L$_{175}$-1	98.4	98.4	2.54	2.60	113.1	115.0	27.59	26.43	Bar Fracture
F-G$_6$L$_{175}$-2	94.7	(3.02)	2.33	(0.25)	116.6	(1.44)	29.10	(2.77)	Bar Fracture
F-G$_6$L$_{175}$-3	102.1		2.94		115.3		22.61		Bar Fracture
F-G$_7$L$_{75}$-1	61.1	61.7	1.70	1.64	61.1	61.7	1.80	1.78	Bar bond slip
F-G$_7$L$_{75}$-2	60.1	(1.56)	1.59	(0.05)	60.1	(1.56)	1.67	(0.08)	Bar bond slip
F-G$_7$L$_{75}$-3	63.8		1.62		63.8		1.86		Bar bond slip
F-G$_7$L$_{125}$-1	99.8	96.7	2.47	2.59	99.8	100.1	6.88	6.66	Bar bond slip
F-G$_7$L$_{125}$-2	94.3	(2.31)	2.41	(0.21)	104.6	(3.56)	6.12	(0.38)	Bar bond slip
F-G$_7$L$_{125}$-3	95.9		2.88		95.9		6.97		Bar bond slip
F-G$_7$L$_{175}$-1	95.8	95.6	2.11	2.18	114.7	115.6	19.64	20.60	Bar Fracture
F-G$_7$L$_{175}$-2	94.1	(1.15)	2.08	(0.12)	116.6	(0.78)	17.95	(2.64)	Bar Fracture
F-G$_7$L$_{175}$-3	96.9		2.35		115.4		24.20		Bar Fracture

* The tensile strength is obtained from the average of tensile strength of three identical specimens.

greater than that of the counterpart control specimen, as the bond strength between the rebar and grout increased due to the confinement effect presented by the properties of the FRP sleeve, such as the number of FRP layers, type of FRP sheet (i.e., Carbon and glass), and bonding characteristics of aluminum and FRP sleeve. Note that the tensile capacity of the FRP sleeve had an essential influence on this issue.

Fig. 10(a) shows the FRP sleeve fracture that occurred in specimens F-C_6L_{125}. Under an average load of 101.1 kN, a partial fracture was observed at the center of the FRP sleeve. In this failure mode, the FRP sleeve exceeded its tensile strength (i.e., 101.1 kN), while the spliced bars did not reach the ultimate tensile strength of the rebar (i.e., 120.2 kN). Such failure occurred because the inadequate number of FRP layers was unable to provide the required radial strength and stiffness to resist the normal splitting stresses generated by radial expansion of the grout.

In specimen F-G_7L_{75}, bar bond-slip failure occurred (Fig. 10(b)). As seen in Table 5, bar bond-slip failure of FRP sleeve specimens occurred at the tensile loads of (56.4 to 106.4) kN. Such failure occurred as the surrounding grout was split by the wedging action of the rebar ribs, and the grout was crushed by pull-out of the ribs. Adequate grout-sleeve bond strength was developed by the corrugated profile of aluminum tube, which prevented the delamination of grout from the sleeve in GSSC. Thus, the grout remained in the sleeve throughout the test. With the combination of corrugated aluminum tube and FRP layers as a means of confinement, the splitting cracks were restrained, but the bond failure occurred by shear failure of the grout keys between rebar ribs. This result indicates that the rebar-grout bond strength developed by the shear resistance of the grout keys is insufficient. After the shear failure of the grout keys, the rebar-grout bond strength was significantly dependent on the friction between the rebar and damaged grout keys.

In general, bond–slip failure of aluminum tube was observed in specimens F-G_6L_{125}. In this case, the corrugated shape of flexible aluminum tube (i.e., F-FRP specimen groups) did not generate the required bond strength between the aluminum tube and surrounding FRP sleeve. As shown in Fig. 10(c), after complete debonding of aluminum tube at the end of the GSSC, the load–displacement behavior of the specimen was similar to that of the control specimens in a brittle manner, with a sudden drop of load. As a result, these specimens failed by the bond–slip failure of aluminum tube before the ultimate tensile strength of the spliced bars. This result indicates that the aluminum tube profile is a critical component to generate the adequate bond mechanism between the aluminum tube and FRP sleeve interface under tensile load.

Although specimens F-C_6L_{125} and F-G_6L_{125} had the same rebar embedded length, different failure modes occurred. Because F-C_6L_{125} used CFRP sheets that had higher tensile strength than GFRP sheets, F-C_6L_{125} failed by sleeve fracture at higher load of 101.1 kN without premature failure. On the other hand, F-G_6L_{125} using CFRP sheets with lower tensile strength failed by premature failure of tube bond slip at lower load of 89.1 kN. For this reason, the GFRP sleeve fracture failure did not occur.

According to previous studies [46,47], the tensile load–displacement behavior of the acceptable GSSC showed three stages: 1) elastic state; 2) rebar yielding; and 3) tensile fracture of spliced bar. Tensile fracture of the spliced bar is a major factor that determines the acceptability of the GSSC. In this type of failure, the ultimate strength of the GSSC was $P_u =$ (113.1 to 119.3) kN, which reached the tensile strength of a single bar (i.e., 118.7 kN) (Table 5). This result indicates that the proposed grouted splice can transfer the tensile load sufficiently to provide continuity of rebars.

3.3. Load-displacement relationships of GSSC

Fig. 11 shows the load–displacement relationship of the representative specimens. Two types of behavior (i.e., ductile mode and brittle failure) were categorized, based on the trend of the load–displacement relationship. Specimens F-C_7L_{175} (i.e., 175 mm embedded length, and seven FRP layers) showed ductile behavior, while specimen groups F-G_7L_{75} (i.e., 75 mm embedded length, and seven FRP layers) and F-C_7L_{125} (i.e., 125 mm embedded length, and seven FRP layers) showed brittle failure. Thus, the embedded length greater than 175 mm is recommended.

Fig. 11(a) shows the load–displacement relationships of specimen group F-C_7L_{175} failed in rebar fracture due to sufficient bond strength. In this figure, the initial slope of the load–displacement relationship is shown as line A-B. The main rebar yielded at the tensile load of about 95 kN. Consequently, the stiffness decreased significantly (i.e., line C–D). By the interception between the two lines A–B and C–D, the yield strength (P_y) and corresponding displacement (d_y) were defined. After yielding, large displacement occurred, due to the plastic elongation of spliced bars. Ultimately, rebar fracture occurred at the outside of the FRP sleeve.

Fig. 11(b) shows the load–displacement relationships of specimen group F-G_7L_{75} failed in bar bond-slip (i.e., brittle manner). Initially, the load–displacement relationships of the specimens were similar to those of the specimens with ductile behavior. However, bond-slip failure occurred before rebar yielding.

Specimen group F-C_7L_{125} showed bar bond-slip failure, which exhibited relatively low ductility (Fig. 11(c)). Specimen group F-C_7L_{125} failed at about 104.7 kN immediately after the yielding of spliced bars. The bond between the rebar and grout failed during the strain hardening process of the spliced bars. For this reason, rebar bond failure occurred after slight rebar elongation.

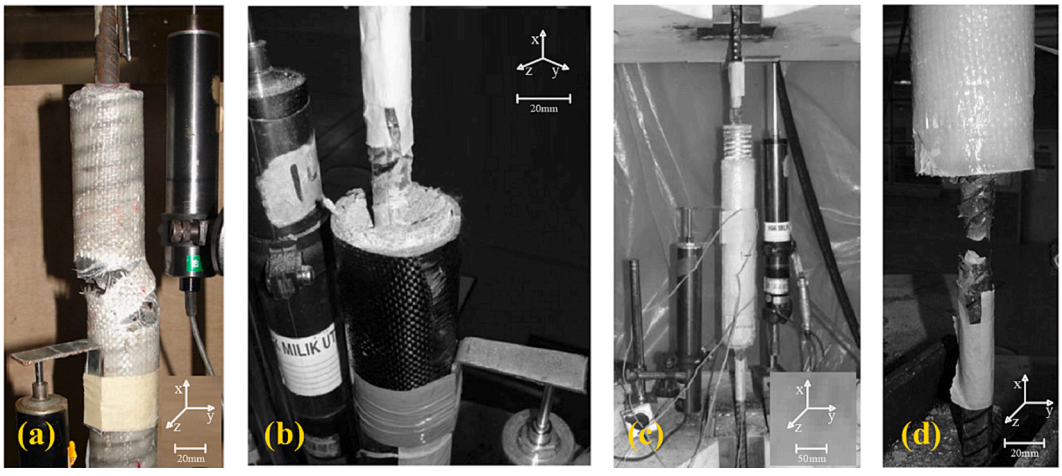

Fig. 10. Failure mode (a) sleeve fracture, F-C_6L_{125}-1; (b) rebar bond–slip failure, F-G_7L_{75}-1; (c) tube bond slip failure, F-G_6L_{125}-1; (d) rebar fracture, F-C_6L_{175}-3.

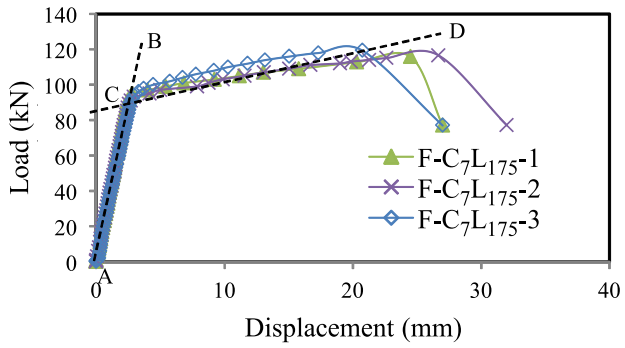

(a) Specimens F-C_7L_{175}

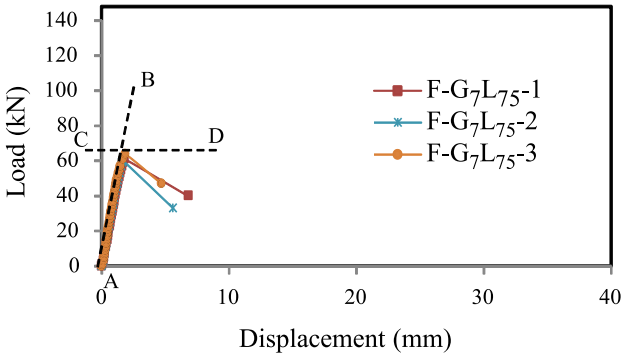

(b) Specimens F-G_7L_{75}

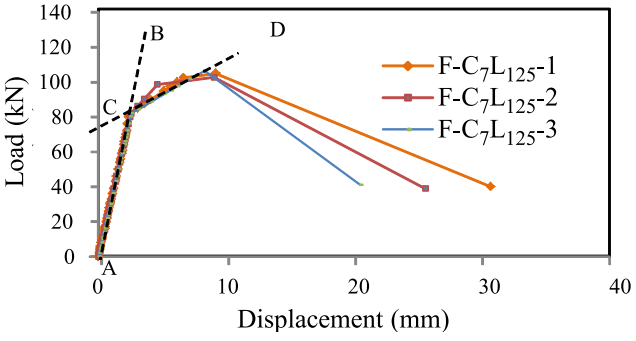

(c) Specimens F-C_7L_{125}

Fig. 11. Load-displacement of the F-G series.

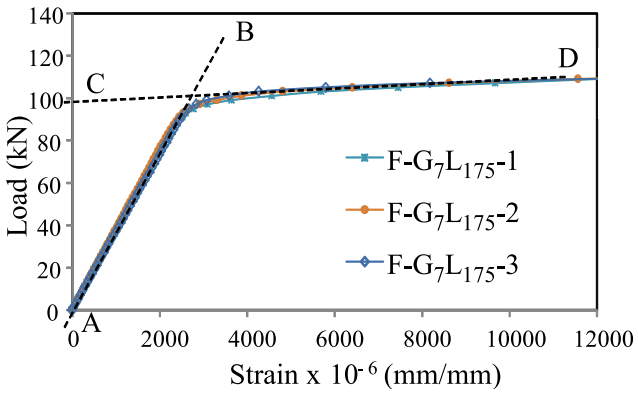

(a) Strain gauge SG1

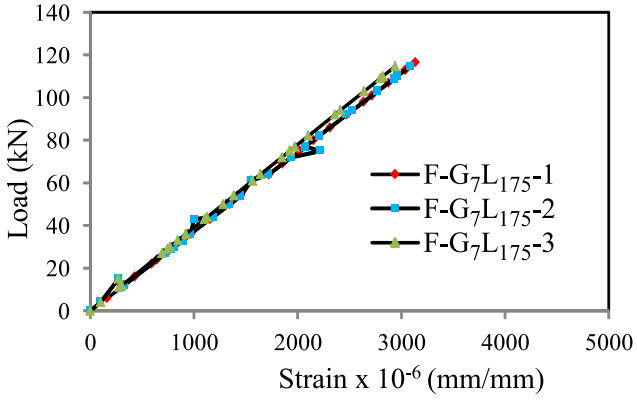

(b) Strain gauge SG2

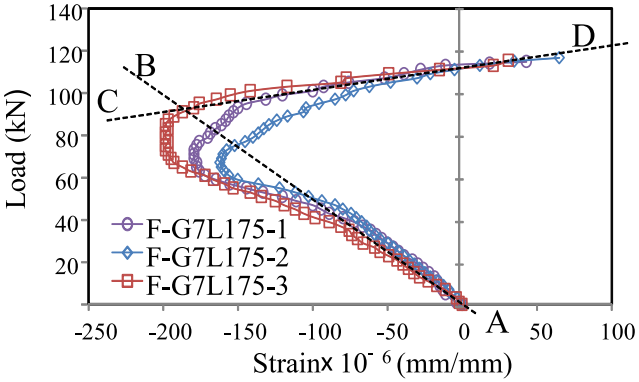

(c) Strain gauge SG3

Fig. 12. Load-strain responses of the F-FRP grouted splices.

3.4. *Strains of rebar and sleeve*

Fig. 12 shows the load–strain relationships at SG1, SG2, and SG3 (refer to Fig. 9), where strain gauges SG1, SG2, and SG3 measure the longitudinal strain of rebar, longitudinal strain of FRP sheet, and transverse or hoop strain of FRP sleeves, respectively. In specimen group F-G_7L_{175} with embedded length of 175 mm, the rebar strain recorded by SG1 exceeded the yield strain of 2,430 $\times$ 10^{-6} mm/mm (Fig. 12(a)). These specimens behaved in two phases: 1) elastic behavior before yielding (i.e., line A-B); and 2) inelastic behavior (i.e., line C-D) with large strains after yielding of the spliced bars. As shown in Fig. 12(b), only small longitudinal strain (i.e., 3,052 $\times$ 10^{-6} mm/mm) developed in the sleeve, compared to the ultimate strain of GFRP composite (i.e., 24,100 $\times$ 10^{-6} mm/mm), indicating that the sleeve did not yield during the test. Thus, adequate thickness of the sleeve was provided. Fig. 12(c) shows the transverse strain of the sleeve. Due to the longitudinal stretching of the grouted splice under tension force, the sleeve shrinks in the transverse direction (i.e., line A–B in Fig. 12(c)). As the tension force increased, due to the splitting expansion of the grout in the sleeve from the surface of the spliced bars, the sleeve expanded. Thus, tensile strain in the transverse direction of the sleeve developed (i.e., line C–D in Fig. 12(c)).

4. Discussion

4.1. *Effect of FRP type*

The bond performance of a GSSC significantly depends on the bond mechanism between the rebar-grout and grout-sleeve interfaces. The bond mechanism between the rebar and grout is mainly affected by the chemical adhesion, frictional resistance between these interfaces, and mechanical interlocking between grout keys and rebar ribs. This

mechanical interlock is obtained by two phenomena: 1) bearing action due to grout shear keys; and 2) confinement action due to radial hoop tension.

Fig. 13 shows that as the pull-out force is applied to the rebar, the reaction forces (R) of the deformed bar can be decomposed into longitudinal (L) and normal (N) component stresses with respect to the rebar axis. The longitudinal component stress (L) is applied to the grout shear key (i.e., ① in Fig. 13), which results in the bearing stress in front of each rebar rib. The grout shear keys restrain the bar-slip by interlocking the ribs along the rebar axis. This mechanism combined with chemical adhesion between the rebar and surrounding grout improves the frictional resistance between the rebar and grout. As the axial tension force increases, the wedging action developed by the rebar ribs increases. When the wedging action surpasses the shear strength, the grout shear keys between rebar ribs are crushed, and pull-out failure occurs.

On the other hand, the applied normal componential stress (N) to the inclined surface of the rebar rib generates reaction of radial confinement stress (M) that confines the grout (see Fig. 14). Afterward, the radial confinement stress generates a compressive region in the grout surrounding rebar. This compressive region generates a uniform compressive field around the spliced bars, which increases the frictional resistance between the rebar and surrounding grout. Depending on the magnitude of the applied load, the grout in compression can decrease the propagation of tensile splitting cracks.

For more explanation of the confinement effect, note that the increased volume of the grout results in the tensile hoop stress (T_S) perpendicular to the radial direction at the grout and sleeve (see Fig. 14). The radial tension in the grout initiates radial cracks, which split the grout along the spliced bars. On the other hand, the sleeve provides the confinement reaction (M), which resists the expansion of the grout and propagation of radial cracks. The propagation of radial cracks and splitting of the grout can be prevented by providing sufficient confinement. When splitting cracks propagate through the entire grout, bond splitting failure occurs. Thus, the bond performance of GSSC is affected by the type of FRP, while different types of FRP make different tensile hoop stress (T_S).

Consequently, flexible corrugated tubes wrapped in CFRP sheets (i.e., F-C specimen groups) achieved higher tensile strengths than corrugated tubes wrapped in GFRP sheets (i.e., F-G specimen groups). As shown in Table 5, this trend was even more evident for the specimens with embedded length of 75 mm. The tensile strength of F-G6 specimen groups with embedded length of 75 mm increased by 16% (i.e., from (59.2 to 68.7) kN when the wrapping material changed from GFRP to CFRP sheets), due to the higher tensile strength and elastic modulus of carbon fiber (i.e., 1,200 MPa) than that of glass fiber (i.e., 700 MPa) (see Table 4).

4.2. Effect of the number of FRP layers

According to the test results, the bond performance of the GSSC is affected by confinement force due to the number of FRP layers (i.e., the confinement). As seen in Table 5, as the number of FRP layers increased, the tensile strength increased slightly (i.e., by (0.5–12.3) % in the glass FRP grouted splices, and by (1.5–3.5)% in the carbon FRP grouted splices) due to the increase of only one layer. However, sufficient FRP layers can enhance the frictional resistance, by controlling the propagation of the splitting cracks around the spliced bars. On the other hand, when the number of FRP layers was insufficient, FRP grouted splices failed in brittle manner near the end or mid-length region, due to the linear-elastic and brittle behavior of FRP wraps (see Fig. 10(a) and Fig. 15). In this case, the FRP sleeve exceeded its ultimate stress, which was not able to provide the required radial strength and stiffness to effectively resist the normal splitting stresses generated by the radial expansion of the grout (see Fig. 15(b)). Thus, the ultimate strength of the spliced bars was not developed.

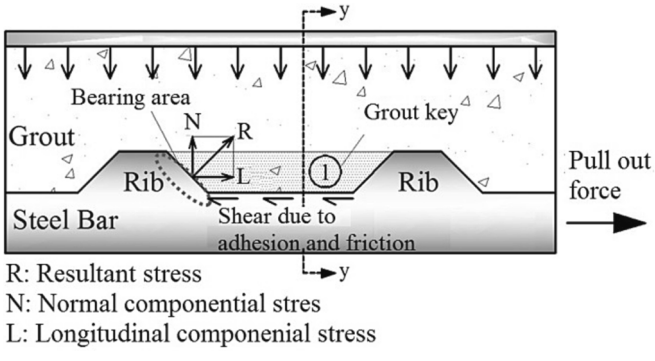

Fig. 13. Mechanical interlocking mechanism of bond and component stresses.

4.3. Effect of embedded length

The test results showed that as the rebar embedded length increased, the ultimate tensile strength of the GSSC increased. Due to the improvement of bond strength, the increased embedded length enhanced the tensile strength of the GSSC, which was also reported in previous study [19]. As the embedded length increases, more grout keys are involved, and smaller stress is applied to each grout key, which reduces the propagation of inclined cracks and the bond strength degradation. For this reason, the ultimate tensile strengths can be increased, due to the increase of interlocking between grout keys and rebar ribs. Table 5 shows that as the embedded length increased from (75 to 175) mm, the average tensile strengths of the grouted splice sleeves using carbon FRP and glass FRP increased by (66.5 and 94.0) %, respectively.

4.4. Feasibility of GSSC

To evaluate the bond performance of the GSSC, the yield ratio (μ_y), strength ratio (μ_s), and ductility ratio (μ_d) were calculated. When μ_y, μ_s, and μ_d satisfy the minimum requirements of the current design codes (e.g., ACI 318–19 [48] and AC-133 [44]), the proposed GSSC can be considered as an adequate GSSC to resist tension force [44,48–50].

The yield ratio (μ_y) of the GSSC is defined as follows:

$$\mu_y = \frac{\sigma_y}{\sigma_{sy}} \geqslant 1.0 \tag{1}$$

where σ_y is the yield strength of the rebar; and σ_{sy} is the specified yield strength. The minimum yield ratio of $\mu_y = 1.0$ indicates that the spliced bar yields in the test specimens.

The strength ratio (μ_s) is defined as follows:

$$\mu_s = \frac{\sigma_u}{\sigma_{sy}} \geqslant 1.25 \tag{2}$$

where σ_u is the ultimate stress of the rebar ($=P_u/A_s$, where P_u is the axial tension force; and A_s is the cross-sectional area of the rebar).

According to ACI 318–19 [48] and AC-133 [44], the acceptable range of the strength ratio is determined as $\mu_s \geq 1.25$ to develop at least 125% of the specified yield strength of the spliced bars.

The ductility ratio (μ_d) is defined as follows:

$$\mu_d = \frac{\Delta_u}{\Delta_y} \geqslant 4.0 \tag{3}$$

where Δ_u is the ultimate displacement corresponding to the peak load; and Δ_y is the yield displacement corresponding to the intersection of lines A-B and C-D in Fig. 11. The ductility ratio μ_d should be greater than 4.0, which is the target ductility ratio to secure life safety in the low-moderate seismic zone, according to design codes and previous studies [47,50–53].

The acceptable indices for the proposed GSSC can be determined as

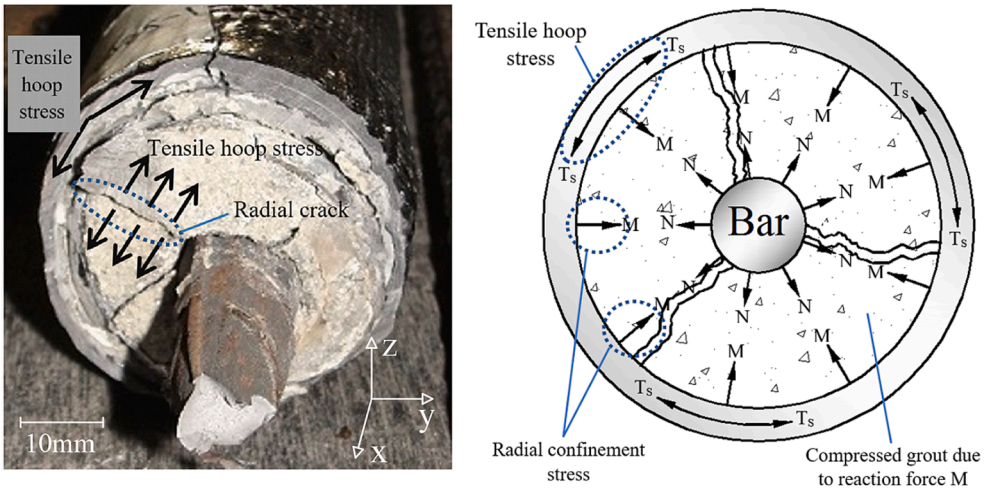

Fig. 14. Mechanism of radial crack propagation and confinement of sleeve.

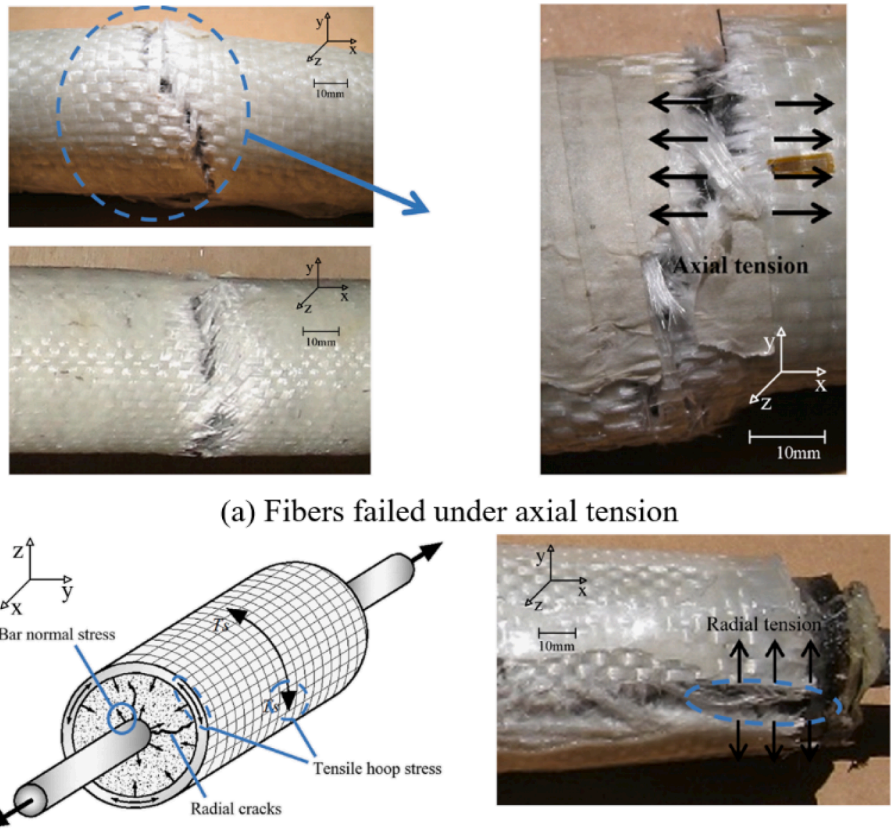

Fig. 15. FRP grouted splices failed under axial and radial tension.

$\mu_y \geq 1.0$, $\mu_s \geq 1.25$, and $\mu_d \geq 4.0$, respectively. Table 6 shows the calculated values of μ_y, μ_s, and μ_d of the GSSC specimens. Regardless of the FRP type and the number of FRP layers, the specimens with embedded length of 175 mm satisfied the bond requirements. Thus, as discussed in the section "**Load-displacement relationships of GSSC**", the embedment length greater than 175 mm is recommended for the proposed GSSC.

5. Analytical model

To predict the tensile strength of GSSC including the confinement effect, an analytical model was developed. Because the actual bond stress distribution along the rebar interface is difficult to measure, a simple assumption of uniform bond stress distribution along the embedded length of the spliced rebar is used [16,54,67], which has generally been used and verified in existing studies with various configurations of grouted sleeves [10,19,55–59]. Further, short rebar embedded lengths of (75, 125, and 175) mm adopted in this study are

Table 6
Feasibility evaluation of test specimens.

Specimen	Ultimate tensile strength P_u(kN)	Ultimate displacement Δ_u(mm)	Yield ratio μ_y	Strength ratio μ_s	Ductility ratio μ_d	Remarks*
F-C_6L_{75}-1	70.1	2.25	0.68	0.75	1.19	NA
F-C_6L_{75}-2	73.1	2.33	0.78	0.78	1.02	NA
F-C_6L_{75}-3	62.9	1.94	0.68	0.68	1.015	NA
F-C_6L_{125}-1	99.1	3.96	0.68	0.68	1.48	NA
F-C_6L_{125}-2	101.3	4.82	0.81	1.09	2.09	NA
F-C_6L_{125}-3	102.9	3.43	0.90	1.11	1.44	NA
F-C_6L_{175}-1	114.8	25.77	1.07	1.25	10.64	A
F-C_6L_{175}-2	113.8	21.95	1.01	1.24	8.67	A
F-C_6L_{175}-3	117.5	17.66	1.02	1.26	7.78	A
F-C_7L_{75}-1	68.5	2.16	0.70	0.73	1.16	NA
F-C_7L_{75}-2	74.2	2.34	0.72	0.80	1.25	NA
F-C_7L_{75}-3	68.4	2.15	0.73	0.73	1.04	NA
F-C_7L_{125}-1	105.0	8.95	1.22	1.15	4.06	NA
F-C_7L_{125}-2	102.7	8.83	1.02	1.1	3.47	NA
F-C_7L_{125}-3	106.4	8.12	1.00	1.15	3.70	NA
F-C_7L_{175}-1	115.8	24.51	1.02	1.25	9.42	A
F-C_7L_{175}-2	116.6	26.66	1.01	1.26	10.1	A
F-C_7L_{175}-3	119.3	20.77	1.04	1.28	7.28	A
F-G_6L_{75}-1	60.1	1.83	0.41	0.64	1.02	NA
F-G_6L_{75}-2	56.4	1.79	0.60	0.60	1.02	NA
F-G_6L_{75}-3	61.1	1.83	0.65	0.66	1.18	NA
F-G_6L_{125}-1	89.0	2.82	0.72	0.96	1.48	NA
F-G_6L_{125}-2	90.2	2.91	0.83	0.97	1.54	NA
F-G_6L_{125}-3	88.0	3.03	0.74	0.95	1.53	NA
F-G_6L_{175}-1	113.1	27.59	1.07	1.25	10.86	A
F-G_6L_{175}-2	116.6	29.1	1.01	1.25	12.49	A
F-G_6L_{175}-3	115.3	22.61	1.02	1.26	7.70	A
F-G_7L_{75}-1	61.1	1.8	0.65	0.65	1.05	NA
F-G_7L_{75}-2	60.1	1.67	0.64	0.64	1.05	NA
F-G_7L_{75}-3	63.8	1.86	0.68	0.68	1.14	NA
F-G_7L_{125}-1	99.8	6.88	1.07	1.07	1.16	NA
F-G_7L_{125}-2	104.6	6.12	1.05	1.13	2.45	NA
F-G_7L_{125}-3	95.9	6.97	0.94	1.03	1.17	NA
F-G_7L_{175}-1	114.7	19.64	1.03	1.23	9.3	A
F-G_7L_{175}-2	116.6	17.95	1.01	1.25	8.6	A
F-G_7L_{175}-3	115.4	24.2	1.04	1.24	10.3	A

* A: Acceptable; NA: Not Acceptable.

within the range where the actual bond stress distribution can be assumed uniform [65,66]. For this reason, the average bond stress in **Eq. (4)** can be used to predict the bond strength of the GSSC. The relationship between the bond force of bar splices (P_u) and the average bond stress of the rebar (τ) can be defined as follows [60]:

$$P_u = \pi d_b L_e \tau \tag{4}$$

where d_b is the diameter of the spliced bar; and τ is the average bond stress of the spliced bar, which can be derived as follows [5]:

$$\tau = (C + D\sqrt{\sigma_{n,b}})\sqrt{f_g'} \tag{5}$$

where C and D are constants related to the type of sleeve; $\sigma_{n,b}$ is the average confinement stress of the grout acting on the spliced steel rebar; and f_g' is the compressive strength of the grout (i.e., 60 MPa in this study).

Based on the previous research [56,57], the confinement force acting on the spliced bar can be equivalent to the confinement force initiated by the grouted sleeve. Thus, it is assumed that the confinement stress of the FRP sleeve acting on the grout can be uniform along the embedded length of the spliced bar, without consideration of the effects of local confinement stress and bond strength generated by different configurations of the sleeves [10,57,61,62].

Based on the test results, the confinement stress of the sleeve and the longitudinal tensile strength of the FRP GSSC were predicted. According to the free body diagram (Fig. 16) proposed by Einea [10], the confinement stress (σ_n) in the sleeve can be calculated from the transverse tensile stress developed in the sleeve ($\sigma_{T,sl}$).

The transverse tensile stress of the sleeve ($\sigma_{T,sl}$) was defined as follows:

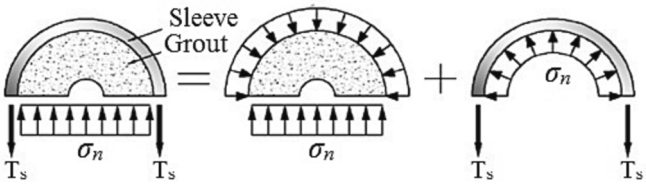

Fig. 16. Free body diagram of stress in the GSSC proposed by Einea [10].

$$\sigma_{T.sl} = \varepsilon_{T,sl} E_{sl} \tag{6}$$

where $\varepsilon_{T,sl}$ is the tensile strain measured at the sleeve (refer to Table 7 and Fig. 17); and E_{sl} is the elastic modulus of the sleeve (i.e., 125,000 MPa for CFRP, and 29,000 MPa for GFRP in this study, see Table 4).

Table 7
Comparisons between the predicted ultimate tensile strength and test results.

Specimens	$\varepsilon_{T,sl}$ (mm/mm × 10^{-6})	$P_{u,pred}$ (**Eq. (14)**)	$P_{u,\exp}$	$P_{u,pred}$ / $P_{u,\exp}$
F-C_6L_{75}	48	66.8	68.7	0.97
F-C_6L_{175}	3	117.1	115.4	1.01
F-C_7L_{75}	52	70	70.4	1.00
F-C_7L_{125}	34	108.6	108.0	1.01
F-C_7L_{175}	5	120.4	117.2	1.03
F-G_6L_{75}	214	68.1	59.2	1.15
F-G_6L_{175}	15	116.5	115.0	1.01
F-G_7L_{75}	240	71.2	61.7	1.15
F-G_7L_{125}	69	97.4	100.1	0.97
F-G_7L_{175}	46	129.7	115.6	1.12

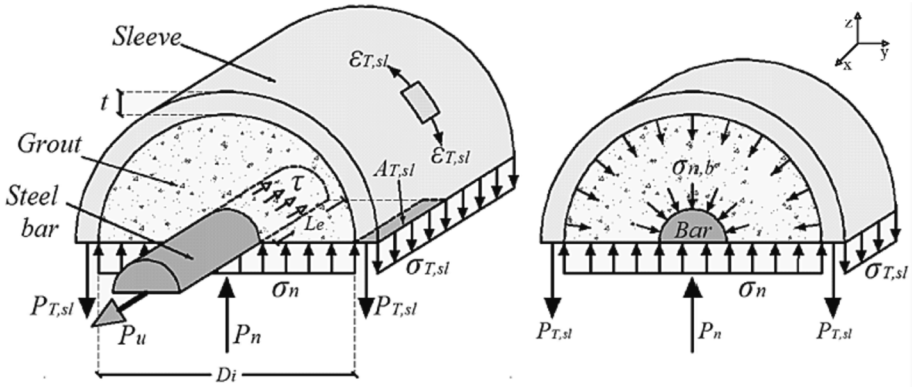

Fig. 17. Free body diagram of stress of the FRP grouted splice connection.

The transverse tensile stress ($\sigma_{T,sl}$) is obtained by dividing the transverse tensile force ($P_{T,sl}$) by the effective transverse cross-sectional area of the sleeve ($A_{T,sl}$), which is defined as a function of the sleeve thickness (t_{sl}) and the effective confinement length equivalent to the rebar embedded length (L_e).

$$\sigma_{T,sl} = \frac{P_{T,sl}}{A_{T,sl}} = \frac{P_{T,sl}}{L_e t_{sl}} \tag{7}$$

The transverse tensile force of the sleeve ($P_{T,sl}$) that introduces confinement stress to the GSSC can be determined from **Eqs. (6) and (7)**.

$$P_{T,sl} = \varepsilon_{T,sl} E_{sl} L_e t_{sl} \tag{8}$$

In the free body diagram introduced by Einea [10] (see Fig. 16), the normal confinement stress introduced by the sleeve (σ_n) can be defined from the static equilibrium condition.

$$\sigma_n = \frac{2P_{T,sl}}{D_i L_e} \tag{9}$$

where D_i is the diameter of sleeve.

Substituting $P_{T,sl}$ of **Eq. (8)** into **Eq. (9)**, σ_n can be re-defined as follows:

$$\sigma_n = \frac{2\varepsilon_{T,sl} E_{sl} t_{sl}}{D_i} \tag{10}$$

To quantify the normal confinement stresses ($\sigma_{n,b}$) acting on the surface area along the rebar embedded length in cylindrical grouted splices, the equivalent normal confinement force (P_n) is divided by the contact surface area ($A_{b,p}$) of the rebar.

$$\sigma_{n,b} = \frac{P_n}{A_{b,p}} = \frac{\sigma_n(\pi D_i L_e)}{\pi d_b L_e} = \frac{\sigma_n D_i}{d_b} \tag{11}$$

To predict the tensile strength of the GSSC, the relationship between the confinement stress ($\sigma_{n,b}$) and bond stress (τ) was considered. Fig. 18 shows the relationship between the normalized bond stress ($\tau/\sqrt{f_g'}$) and normal confinement stress ($\sqrt{\sigma_{n,b}}$) according to the method proposed by Untrauer and Henry [5] for the GSSC specimens showing the bar bond-slip or bar fracture.

In Fig. 18, the bond stress (τ) can be defined as a function of the confinement stress ($\sigma_{n,b}$) and grout strength (f_g'). The values of C and D in **Eq. (5)** were determined as (1.546 and 0.493) by linear regression analysis of the present test results.

$$\tau = \left(0.493\sqrt{\sigma_{n,b}} + 1.546\right)\sqrt{f_g'} \tag{12}$$

Substituting **Eq. (12)** into **Eq. (4)**, the ultimate tensile strength (P_u) of the GSSC is calculated as follows:

$$P_u = \pi d_b L_e \left(0.493\sqrt{\sigma_{n,b}} + 1.546\right)\sqrt{f_g'} \tag{13}$$

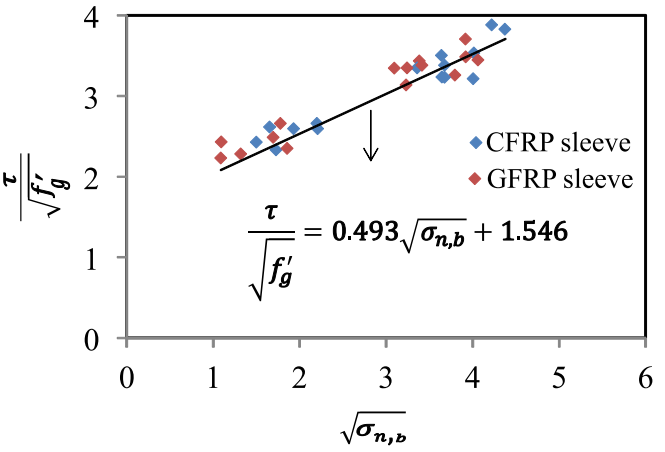

Fig. 18. Relationship between $\tau/\sqrt{f_g'}$ and $\sqrt{\sigma_{n,b}}$.

As the confinement stress ($\sigma_{n,b}$) in Eq. (13) is difficult to quantify in practice, substituting Eqs. **(10) and (11)** into Eq. (13) further simplifies P_u, as follows:

$$P_u = \pi d_b L_e \left(0.493\sqrt{\frac{2\varepsilon_{T,sl} E_{sl} t_{sl}}{d_b}} + 1.546\right)\sqrt{f_g'} \tag{14}$$

When the ultimate tensile strength (P_u) of the GSSC calculated by **Eq. (14)** is greater than the ultimate tensile strength of rebar, the rebar fracture would occur. However, according to the test results of this study, the peak load of the specimens governed by rebar fracture was slightly less than the ultimate tensile strength of the rebar. Due to bond-slip of the longitudinal bar developed in the micro-space between the surrounding grout keys and rebar ribs, the grout was radially dilated, which decreased the effective ultimate tensile strength.

Based on the test results, the reduction coefficient of tensile capacity (α) is suggested as follows:

$$\alpha = \frac{P_j}{P_c} \tag{15}$$

where P_j is the measured ultimate tensile strength of test specimens with bar fracture failure; and P_c is the measured ultimate tensile strength of the rebar.

Thus, the effective tensile strength of the spliced bar (F_b) can be defined as follows:

$$F_b = \alpha P_c \tag{16}$$

As shown in Fig. 19, the average tensile strength of specimen with bar fracture failure is $P_j = 115.8$ kN, while the measured tensile strength

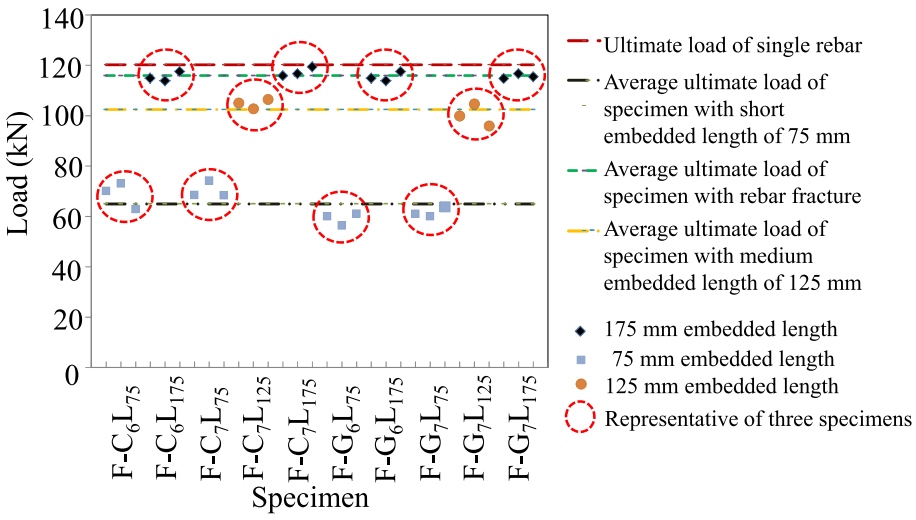

Fig. 19. Tensile resistance of specimen groups.

of the rebar is $P_c = 120.2$ kN. Thus, the corresponding reduction coefficient α is calculated as 0.96. Such result would be attributed to bond slip between rebar and grout [63].

The failure mode of the proposed GSSC can be judged using the tensile capacity of the rebar. In the case of $P_u < F_b$, the proposed GSSC fails due to bar-slip. In the case of $P_u \geq F_b$, the proposed GSSC can transfer the tensile force until rebar fracture.

Table 7 presents the predicted tensile strengths of the specimens calculated by **Eq. (14)**. The proposed model **(Eq. (14))** predicted the test results well, showing the average ratio of predictions to test results = 1.04 and COV. = 0.064. This result indicates that the ultimate tensile strength of the GSSC can be predicted using the confinement stress developed by the sleeve. However, note that the predicted values given in Table 7 are dependent on the transverse strain obtained from the experiments, which implies a drawback of **Eq. (14)**, as it relies on the experimental data. Thus, further studies are needed to define the transverse strain in practice. One of the approaches is to estimate the transverse strain by conducting analytical studies on numerous GSSC specimens using finite element analysis or Gaussian Quadrature method [68]. Based on the analytical responses of transverse strain, an equation for the corresponding transverse strain to predict the tensile strength of GSSC including the confinement effect can be developed.

Despite the prediction accuracy, some differences of ultimate tensile strength between the predictions and test results would be attributed to the ultimate tensile strength of the GSSC that relies on the interlocking mechanism between 1) shear keys of the deformed bar and surrounding grout, and 2) shear keys of the corrugated aluminum tube and grout. This interlocking mechanism relies on the grout strength that would vary slightly from sample to sample of GSSC, compared to the theoretical method where only one consistent value of grout strength is adopted. To minimize this difference, specimens need to be carefully manufactured and tested to ensure that all samples have the same age of grout and subsequently similar grout strength.

Table 7 shows the specimens that failed by either bar fracture or bar-slip (see Table 5). In a word, specimens F-C6L125 and F-G6L125 and GSSC without FRP sheets are excluded, because these specimens failed by sleeve fracture that are not governed by the bond strength between interfaces 1 and 2 (see Fig. 19). For this reason, the proposed model (**Eq. (14)**) is only applicable to predict the ultimate tensile strength based on the bond strength at interfaces 1 and 2 only (see Fig. 19), assuming the tensile strength of aluminum and FRP composites is sufficient to resist the rebar tensile strength. Further, the proposed model is limited to predict the ultimate tensile strength of the proposed GSSC without incorporating the influence of environmental conditions, such as temperature and moisture.

MC1990 [64] states that the rebar diameter, type of rib, diameter of sleeve, and compressive strength of grout would influence the degree of confinement stress, and thus the tensile capacity of the grouted sleeves. In this study, only the embedded length and sleeve configuration were considered in the analytical model. Thus, further studies are needed to evaluate the effect of various test parameters on the tensile capacity of the grouted sleeves.

5.1. *Load transfer mechanisms of the proposed GSSC*

Fig. 20 shows two discontinuous rebars connected by the proposed GSSC. The success of GSSC is demonstrated by the connection that can transmit the tensile load between rebars without any failure at any interfaces inside the sleeve except the rebar fracture outside the sleeve (Fig. 10(d)). Such rebar fracture indicates that the bond strength at all interfaces is greater than the rebar tensile strength. In the load transfer, the following interfaces inside the sleeve can be considered: at the interface 1, bond failure between the deformed bar and surrounding grout results in rebar pull-out failure (Fig. 10(b)); at the interface 2, bond failure between the grout and inner surface of corrugated aluminum tube results in grout pull-out failure; and at the interface 3, adhesive bond (provided by the epoxy resin) failure between the outer surface of corrugated aluminum tube and FRP sheet results in aluminum tube pull-out failure (Fig. 10(c)). Further, when the number of FRP layers are insufficient, the aluminum and FRP composites would be fractured (Fig. 10(a)).

6. Conclusion

In the present study, 45 GSSC specimens using FRP (i.e., CFRP and GFRP) were tested under monotonic uni-axial tensile load to investigate the effects of embedded length and FRP properties on the feasibility and bond behavior of the GSSC. On the basis of the test results, the following fundamental conclusions have been drawn:

1. When the rebar embedded length was the same, the tensile strength of GSSC with CFRP sheets was greater than that of GSSC with GFRP sheets. This trend was clearly shown in the specimens with embedded length of 75 mm. The tensile strength of the F-G6 specimen group with embedded length of 75 mm increased by 16%, due to the higher tensile strength of carbon (i.e., 1,200 MPa) in comparison to glass (i.e., 700 MPa).

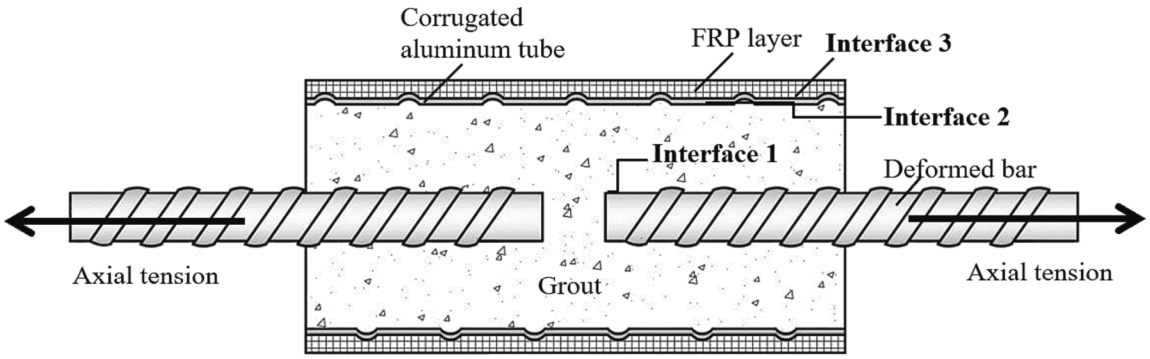

Fig. 20. Load transfer through bond mechanisms.

2. The increased number of FRP layers of the sleeve improved the confinement of the grouted splices. However, due to the increase of only one layer (i.e., six to seven layers), the increase rate of the tensile strength of the FRP grouted splices was not significant: (0.5 – 12.3) % for glass FRP, and (1.5 – 3.5) % for carbon FRP.
3. As the rebar embedded length increased, the ultimate tensile strength of the grouted splice connections significantly increased. As the embedded length increased from (75 to 175) mm, the average tensile strengths of the grouted splices increased by (66.5 – 94.0) %. The increase rate of the tensile strength was greater in the specimens with GFRP (i.e., 94.0 %), compared to the specimens with CFRP (i.e., 66.5%).
4. Based on the acceptable requirements of the yield ratio (μ_y), strength ratio (μ_s), and ductility ratio (μ_d), use of the embedded length of at least 175 mm is recommended in the proposed GSSC, regardless of the FRP type and the number of FRP layers.
5. The ultimate tensile strength of the grouted splice was proposed. The predictions of the proposed method matched well with the experimental ultimate tensile strength of the grouted splices, showing the average ratio of predictions to test results = 1.04 and COV. = 0.064.

It is noted that further studies are needed as follows: 1) the bond strength between the outer surface of FRP sheets and surrounding concrete needs to be investigated; 2) tensile test needs to be performed on aluminum tubes wrapped with FRP sheets to determine the tensile strength of the aluminum tube and FRP sheet composites; and 3) flexural beam test of GSSC connection is needed to investigate the effect of flexural behavior on the splice connections of beams.

CRediT authorship contribution statement

Kiarash Koushfar: Methodology, Writing – original draft, Formal analysis. **Ahmad Baharuddin Abd. Rahman:** Conceptualization, Project administration. **Seyed Jamal Aldin Hosseini:** Writing – original draft, Visualization. **Sung-Hyun Kim:** Writing – review & editing. **Lila Soufia:** Investigation, Visualization. **Yusof Ahmad:** Data curation, Validation. **Su-Min Kang:** Validation. **Yun Zhou:** Validation. **Jong-Min Lee:** Investigation, Data curation. **Hyeon-Jong Hwang:** Methodology, Data curation, Writing – review & editing, Project administration.

Declaration of Competing Interest

The authors declare that they have no known competing financial interests or personal relationships that could have appeared to influence the work reported in this paper.

Data availability

Data will be made available on request.

Acknowledgement

This research was financially supported by the National Research Foundation of Korea (NRF) grant funded by the Korea government (MSIT) (No. 2021R1A4A3030117), Human Resources Development Program of the Korea Insitute of Energy Technology Evaluation and Planning(KETEP) grant funded by the Ministry of Trade, Industry and Energy, Republic of Korea (No. RS-2023-00237035), and the Universiti TeknologiMalaysia (UTM). The authors are grateful for their support of the authorities.

References

[1] Elliott KS. Precast concrete structures. CRC Press; 2016.
[2] Tullini N, Minghini F. Grouted sleeve connections used in precast reinforced concrete construction–Experimental investigation of a column-to-column joint. Eng Struct 2016 Nov;15(127):784–803.
[3] M. K. Thompson, J. O. Jirsa, J. E. Breen, and R. E. Klingner., Anchorage behavior of headed reinforcement: Literature review. Research Report 1855-1, Texas Department of Transportation, 2002.
[4] Pfister JF. Influence of ties on the behavior of reinforced concrete columns. Journal Proceedings 1964.
[5] Untrauer RE, Henry RL. Influence of normal pressure on bond strength. ACI Struct J 1965;62(5):577–85.
[6] Robins P, Standish I. The influence of lateral pressure upon anchorage bond. Mag Concr Res 1984;36(129):195–202.
[7] Moosavi M, Jafari A, Khosravi A. Bond of cement grouted reinforcing bars under constant radial pressure. Cement and Concrete Composites 2005;27(1):103–9.
[8] Alavi-Fard M, Marzouk H. Bond of high-strength concrete under monotonic pull-out loading. Mag Concr Res 2004;56(9).
[9] Soroushian P, Choi KB, Park GH, Aslani F. Bond of deformed bars to concrete: effects of confinement and strength of concrete. ACI Materials Journal 1991;88(3):227–32.
[10] Einea A, Yamane T, Tadros MK. Grout-filled pipe splices for precast concrete construction. PCI J 1995;40(1):82–93.
[11] Loh HY. Development of grouted splice sleeve and its performance under axial tension. Universiti Teknologi Malaysia; 2008.
[12] Loo GK. Parametric study of grout-filled splice sleeve integrated with flexible aluminium tube for precast concrete connection. Universiti Teknologi Malaysia; 2009.
[13] Hosseini SJA, Abd Rahman AB. Effects of spiral diameter on the bond stress– slip relationship in grouted sleeve connector. Malaysian J Civil Eng 2013;12(1).
[14] Hosseini SJA, Abd Rahman AB. Analysis of spiral reinforcement in grouted pipe splices connectors. Gradevinar 2013;65(6).
[15] Hosseini SJA, Abd Rahman AB. Effects of spiral confinement to the bond behavior of deformed reinforcement bars subjected to axial tension. Engineering Structure, Elsevier 2016;112:1–13.
[16] Hosseini SJA, Abd Rahman AB, Osman Mohd Hanim, Saim Aziz, Adnan Azlan. Bond behavior of spirally confined splice of deformed bars in grout, Construction and Building Materials. Elsevier; 2015. p. 180–94.
[17] Hosseini SJA, Abd Rahman AB, Hwang H-J, Hosseinid SK. Su-Min Kang. Bond behavior of spirally confined bar splices in grout. Constr Build Mater 2022;327.
[18] Tibbetts AJ, Oliva MG, Bank LC. Durable fiber reinforced polymer bar splice connections for precast concrete structures. Composites & ploycon 2009:15–7.
[19] Ling JH, Rahman AB, Ibrahim IS. Feasibility study of grouted splice connector under tensile load. Constr Build Mater 2014;15(50):530–9.
[20] Jansson PO. Evaluation of grout-filled mechanical splices for precast concrete construction. Michigan Department of Transportation MDOT; 2008.
[21] Coogler KL, Harries KA, Gallick M. Experimental study of offset mechanical lap splice behavior. ACI Struct J 2008;105(4):478.
[22] TokyoSteelCorp, Tokyo Steel Corp. BCJ-C1659, 1994.

[23] St John NA, Brown JR. Flexural and interlaminar shear properties of glass-reinforced phenolic composites. Compos A Appl Sci Manuf 1998;29(8):939–46.
[24] Callus PJ, Mouritz AP, Bannister MK, Leong KH. Tensile properties and failure mechanisms of 3D woven GRP composites. Compos A Appl Sci Manuf 1999;30(11):1277–87.
[25] Degallaix G, Hassaïni D, Vittecoq E. Cyclic shearing behaviour of a unidirectional glass/epoxy composite. Int J Fatigue 2002;24(2–4):319–26.
[26] Vlot A, Gunnink JW, editors. Fibre metal laminates: an introduction. Springer Science & Business Media; 2011.
[27] Tarnopol'skii YM, Arnautov AK, Kulakov VL. Methods of determination of shear properties of textile composites. Compos A Appl Sci Manuf 1999;30(7):879–85.
[28] Rikards R. Interlaminar fracture behaviour of laminated composites. Comput Struct 2000;76(1–3):11–8.
[29] Kawai M, Hachinohe A, Takumida K, Kawase Y. Off-axis fatigue behaviour and its damage mechanics modelling for unidirectional fibre–metal hybrid composite: GLARE 2. Compos A Appl Sci Manuf 2001;32(1):13–23.
[30] Soprano A, Apicella A, D'Antonio L, Schettino F. Application of durability analysis to glare aeronautical components. Int J Fatigue 1996;18(4):265–72.
[31] Uenal O, Barnard DJ, Anderson IE. A shear test method to measure shear strength of metallic materials and solder joints using small specimens. Scr Mater 1999;40(3).
[32] Chiang MY, He J. An analytical assessment of using the losipescu shear test for hybrid composites. Compos B Eng 2002;33(6):461–70.
[33] Kawai M, Morishita M, Tomura S, Takumida K. Inelastic behavior and strength of fiber-metal hybrid composite: Glare. Int J Mech Sci 1998;40(2–3):183–98.
[34] Naboulsi S, Mall S. Thermal effects on adhesively bonded composite repair of cracked aluminum panels. Theor Appl Fract Mech 1997;26(1):1–2.
[35] Asnafi N, Langstedt G, Andersson CH, Östergren N, Håkansson T. A new lightweight metal-composite-metal panel for applications in the automotive and other industries. Thin-Walled Struct 2000;36(4):289–310.
[36] Asundi A, Choi AY. Fiber metal laminates: an advanced material for future aircraft. J Mater Process Technol 1997;63(1–3):384–94.
[37] Wittenberg TC, Van Baten TJ, De Boer A. Design of fiber metal laminate shear panels for ultra-high capacity aircraft. Aircr Des 2001 Jun 1;4(2–3):99–113.
[38] Vlot A, Gunnink JW, editors. Fibre metal laminates: an introduction. Springer Science & Business Media; 2011.
[39] Vlot A, Fredell RS. Impact damage resistance and damage tolerance of fibre metal laminates. Proceedings of the ICCM/9 Madrid 1993;6:51–8.
[40] Botelho EC, Silva RA, Pardini LC, Rezende MC. A review on the development and properties of continuous fiber/epoxy/aluminum hybrid composites for aircraft structures. Mater Res 2006;9(3):247–56.
[41] Koushfar K. Development of durable fiber reinforcement polymer grouted splice connection. Universiti Teknologi Malaysia; 2011. Master thesis.
[42] Koushfar K, Abd Rahman AB, Ahmad Y, Mohd, Osman H. Bond behavior of the reinforcement bar in glass fiber-reinforced polymer connector. GRADEVINAR 2014;66(4).
[43] ASTM D3039/D3039M-14 Standard Test Method for Tensile Properties of Polymer Matrix Composite Materials. 2014, ASTM International.
[44] AC-133. Acceptance criteria for mechanical connector systems for steel reinforcing bars. ICC Evaluation Service, Inc.; 2008.
[45] ASTM A1034 / A1034M-05, Standard Test Methods for Testing Mechanical Splices for Steel Reinforcing Bars. 2005, ASTM International: West Conshohocken, PA.
[46] Ling JH. Behavior of grouted splice connections in precast concrete wall subjected to tensile, shear and flexural loads. Universiti Teknologi Malaysia; 2011.
[47] Lee GS. Parametric studies of sleeve connector using steel pipe with spiral steel for precast concrete connection. Universiti Teknologi Malaysia; 2009.
[48] ACI CODE-318-19(22): Building Code Requirements for Structural Concrete and Commentary (Reapproved 2022).
[49] Alias A, Zubir MA, Shahid KA, Rahman AB. Structural performance of grouted sleeve connectors with and without transverse reinforcement for precast concrete structure. Procedia Eng 2013;1(53):116–23.
[50] Soudki KA. Behaviour of Horizontal Connections for Precast Concrete Load-bearing Shear Wall Panels Subjected to reversed Cyclic Deformations. University of Manitoba; 1994. PhD.
[51] BS8110 BS. Structural use of concrete, part 1–code of practice for design and construction. British Standards Institution, UK. 1997.
[52] Soudki SHR, LeBlanc B. Horizontal Connections for Precast Concrete Shear Wall Subjected to Cyclic Deformations Part 1: Mild Steel Connections. PCI J 1995;41(1):78–96.
[53] Englekirk RE. Seismic Design of Reinforced and Precast Concrete Buildings. John Wiley & Sons, Inc.; 2003.
[54] Cairns J, Plizzari GA. Towards a harmonised European bond test. Mater Struct 2003;36(8):498–506.
[55] Henin E, Morcous G. Non-proprietary bar splice sleeve for precast concrete construction. Eng Struct 2015;83:154–62.
[56] Zheng YF, Guo ZX, Liu JB, Chen XN, Xiao QD. Performance and confining mechanism of grouted deformed pipe splice under tensile load. Adv Struct Eng 2016;19(1):86–103.
[57] Ling JH, Abd Rahman AB, Ibrahim IS, Hamid ZA. Tensile capacity of grouted splice sleeves. Eng Struct 2016;111:285–96.
[58] Ling JH, Abd Rahman AB, Ibrahim IS, Hamid ZA. Behaviour of grouted pipe splice under incremental tensile load. Constr Build Mater 2012;33:90–8.
[59] Ling JH, Abd Rahman AB, Ibrahim IS, Hamid ZA. An Experimental study of welded bar sleeve wall panel connection under tensile, shear, and flexural loads. International Journal of Concrete Structures and Materials 2017;11(3):525–40.
[60] ACI-116. Cement and concrete terminology ACI 116R-00 2000.
[61] Huang Y, Zhu ZG, Naito CJ, Yi WJ. Tensile behavior of half grouted sleeve connections: experimental study and analytical modeling. Constr Build Mater 2017;152:96–104.
[62] Kim H. Bond strength of mortar-filled steel pipe splices reflecting confining effect. J Asian Archit Build 2012;11(1):125–32.
[63] Lin F, Wu XB. Mechanical performance and stress–strain relationships for grouted splices under tensile and cyclic loadings. Int J Concr Struct Mater 2016;10(4):435–50.
[64] CEB–FIP, 'Model Code 1990', p. 437, Thomas Telford, London 1993, ISBN 0 7277 1696.
[65] Eligehausen, R., E.P. Popov, and V.V. Bertero.Local bond stress-slip relationships of deformed bars under generalized excitations. 1982.
[66] Soroushian P, Choi K-B. Local bond of deformed bars with different diameters in confined concrete. ACI Struct J 1989;86(2).
[67] American Concrete Insitute. Mechanical Connections of Reinforcing Bars.ACI 439. 1991.
[68] Mousavi SE, Sukumar N. Generalized Gaussian quadrature rules for discontinuities and crack singularities in the extended finite element method. Comput Methods Appl Mech Eng 2010;199(49–52):3237–49.